

Characteristics of the Short-Period *S*-Wave Attenuation Field in the Source Zone of the Strongest Tohoku Earthquake of March 11, 2011 ($M_w = 9.0$)

Yu. F. Kopnichev^{a, *} and I. N. Sokolova^b

^a*Schmidt Institute of Physics of the Earth, Russian Academy of Sciences, Moscow, 123242 Russia*

^b*Institute of Geophysical Research of Ministry of Energy of Republic Kazakhstan, Almaty, 050020 Kazakhstan*

*e-mail: yufk777@mail.ru

Abstract—The characteristics of the short-period *S*-wave attenuation field in the source zone of the strongest Tohoku earthquake of March 11, 2011 in the northeast of Japan are considered ($M_w = 9.0$). The records of shallow local earthquakes obtained by the MAJO station at distances of 250 to 700 km are processed. A method based on the analysis of the ratio of the maximum amplitudes of the S_n and P_n waves (the S_n/P_n parameter) is used. The source zone is divided into four regions bounded by coordinates 36° – 37° , 37° – 38° , 38° – 39° , and 39° – $40^\circ 18' N$; and $140^\circ 30'$ – $145^\circ E$. It is established that all the regions contain segments of a rapid decrease in the S_n/P_n values, which are followed by segments of their sharp growth at small epicentral distances in all the areas. Another segment of rapid decrease in the S_n/P_n parameter is identified in all regions at relatively large distances. It is assumed that the first segments of rapid decrease in the S_n/P_n values are related to the gradual sinking of the *S*-wave rays in the mantle wedge. In this case, the minimum values of the parameter correspond to rays partly moving along the foot of this wedge. Such an effect is explained by the fact that the biggest content of the deep-seated fluids ascending due to the dehydration of the oceanic crust rocks correspond to the bottom of the mantle wedge. The segments of a sharp increase in the S_n/P_n values are likely to correspond to the propagation of rays within the upper part of the plate characterized by very weak attenuation. The second segments of the rapid decrease in the S_n/P_n parameter are related to the ray penetration into the waveguide formed in the bottom part of the plate formed as a result of the dehydration of the mantle rocks. The mean values $S_n/P_n(\Delta)$ in the four areas are much lower than in the source zone of the strongest Maule earthquake of February 27, 2010 (Chile, $M_w = 8.8$). This effect agrees with the earlier assumption about the larger fluid content in the subduction zones in the west of the Pacific Ocean compared to the east. Furthermore, this allows us to explain the features of the aftershock processes in these two enormous regions of the Pacific Ring.

Keywords: *S*-waves, attenuation, Tohoku earthquake, deep-seated fluids

DOI: 10.1134/S0001433819080061

INTRODUCTION

The attenuation of short-period *S*-waves is an important characteristic of the medium that carries the information on the content of the liquid phase: fluids or molten rocks (Molnar and Oliver, 1969; Kopnichev, 1985; Kopnichev and Arakelyan 1988). It is shown in (Kopnichev et al., 2009; Kopnichev and Sokolova, 2010a, 2011a, 2011b, 2016) that the regions of the relatively high attenuation of *S*-waves in the lithosphere are formed before numerous strong shallow earthquakes. The available data indicate that these regions correspond to the increased content of deep-seated fluids. At the same time, after strong seismic events, the attenuation in the upper mantle gradually decreases during several decades, which is indicative of the rising mantle fluids (Husen and Kissling, 2001; Kopnichev and Sokolova, 2003; Kopnichev et al., 2009). Therefore, the accumulation of data on the

characteristics of the attenuation field of the *S*-waves in a various areas will probably allow us to use them to identify the source zones of the forthcoming large earthquakes (Kopnichev and Sokolova, 2007, 2010b, 2011b, 2016). In this work, we map the fields of the shear wave attenuation in the source zone of the catastrophic Tohoku earthquake of March 11, 2011 in the northeast of Japan ($M_w = 9.0$).

HISTORICAL SEISMICITY

The characteristics of the attenuation field were studied in the northeast of Japan confined by the coordinates 36° – $40.3^\circ N$ and 140.5° – $145^\circ E$. Here, a series of large earthquakes with $M_w \geq 7.5$ occurred in 1900–2010 (Table 1, Fig. 1). The epicenter of the strongest event (Sanriku, 1933, $M_w = 8.4$) was located in the Pacific Plate region east of the Japan deep

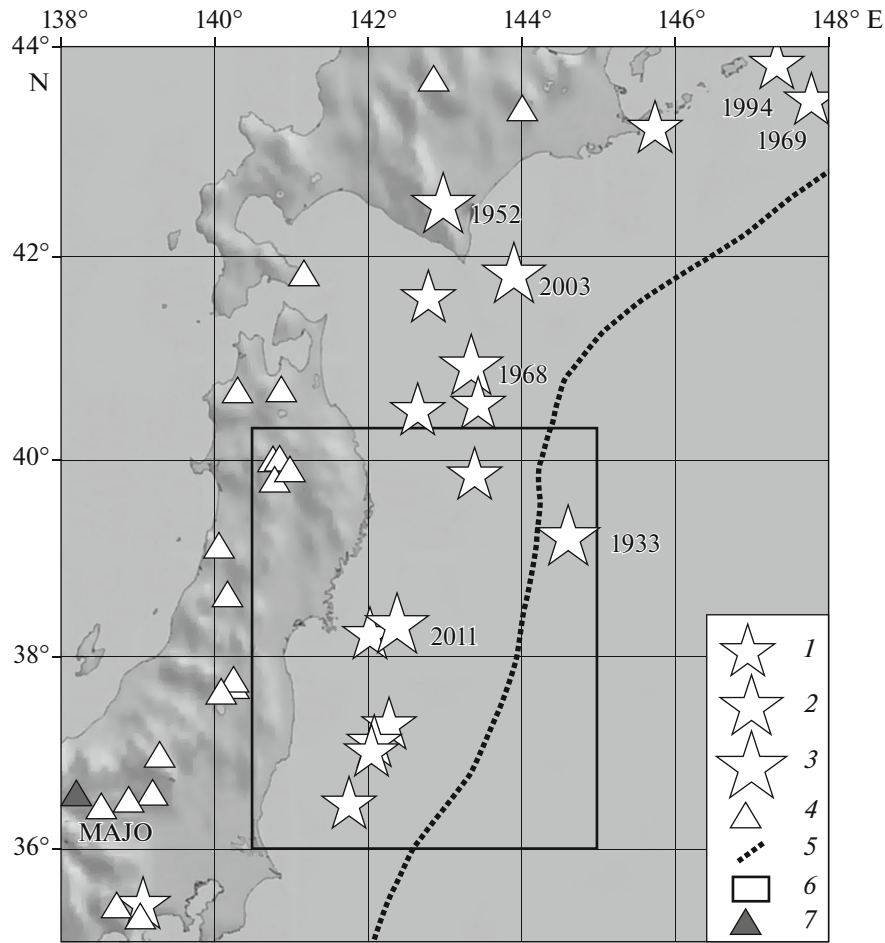


Fig. 1. Chart of the study area. (1–3) Epicenters of large earthquakes. M_w : (1) 7.7–7.9; (2) 8.1–8.4; (3) 9.0. Years are indicated for events with $M_w > 8.0$; (4) volcanoes; (5) axis of the Japan Trench; (6) region of the epicenters for which the seismograms were processed; (7) MAJO seismic station.

trench. West of the trench, only earthquakes with $M_w < 8.0$ were recorded over the stated time; therefore, the strongest Tohoku event of March 11, 2011 was completely unexpected by Japanese seismologists (Goldfinger et al., 2013a). After the revision of the his-

torical data, it was found that the recurrence period of such events can be ~800–1200 years (Goldfinger et al., 2013b). The earthquake generated a strong tsunami that caused many casualties and enormous destruction, including at the Fukushima Nuclear Power Plant. This event was accompanied by many aftershocks (Fig. 2), the strongest of which (in the north of the source zone) had a magnitude of 7.9.

Table 1. Large and great earthquakes in the northeast of Japan from the beginning of XX century between 36° and 41° N

Date	Coordinates, deg		h , km	M_w
	N	E		
Sep. 1, 1923	35.4	139.08	35	7.9
Mar. 2, 1933	39.22	144.62	35	8.4
May 23, 1938	36.46	141.76	35	7.7
Nov. 5, 1938	37.01	142.04	35	7.9
Nov. 5, 1938	37.11	142.08	35	7.8
Nov. 6, 1938	37.29	142.28	35	7.7
Mar. 20, 1960	39.85	143.4	35	7.8
May 16, 1968	40.9	143.35	26	8.3
Jun 12, 1978	38.22	142.02	53	7.7
Mar. 11, 2011	38.32	142.37	32	9.0

MATERIALS AND METHODS

The attenuation field was mapped by the earthquake records obtained at Matsushiro station (MAJO) at distances $\Delta \sim 250\text{--}700$ km (Fig. 1). The station is equipped with an STS1 three-component broad-band seismometer and the digitization frequency is 20 Hz. We selected the data for events with depths of 0 to 33 km from the region bounded by the coordinates 36°–40.3° N and 140.5°–145° E. In total, we processed more than 600 seismograms obtained in 1983–2014. For comparison, we examine the characteristics of the attenuation field in the source zone of the strongest

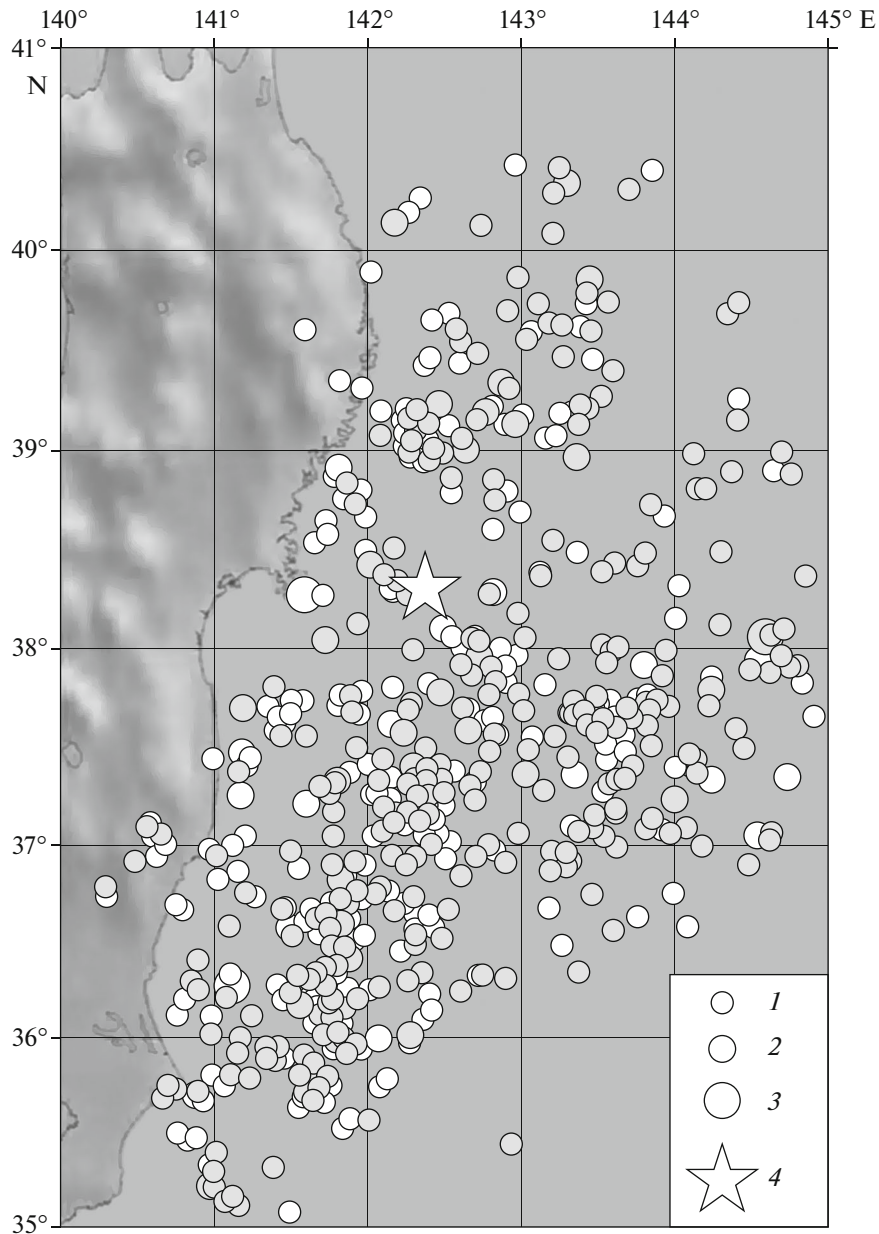


Fig. 2. Aftershocks of the Tohoku earthquake of March 11, 2011. (1–3) Magnitudes: (1) 5.0–5.9; (2) 6.0–6.9; (3) ≥ 7.0 . Filled signs are the depths of 0 to 33 km, white signs are the depths of 34 to 70 km. (4) Is the epicenter of the Tohoku earthquake.

Maule earthquake (Chili, February 27, 2010, $M_w = 8.8$) (Kopnichev and Sokolova, 2011b).

We used the method of mapping an attenuation field in the lithosphere by the ratio of the maximum amplitudes of the S_n and P_n waves' (the $\log(AS_n/AP_n)$ parameter), which for brevity, we designate as S_n/P_n (Molnar and Oliver, 1969; Kopnichev and Arakelyan, 1988; Kopnichev and Sokolova, 2010b, 2011b). Note that some secondary phases (pP , sP , and others) may arrive at regional distances in the near coda wave P_n . However, the P_n waves are manifested at short times most steadily and as a rule have the largest amplitudes.

This also refers to S_n waves (before the arrival of the crustal group Lg). That is why the S_n/P_n parameter has been used for mapping the attenuation field of S-waves in the upper mantle of different continental and oceanic regions for a long time (Molnar and Oliver, 1969; Ni and Barazangi, 1983; Kopnichev and Arakelyan, 1988; Furumura and Kennett, 2001; Zhao et al., 2003; Kopnichev and Sokolova, 2010b, 2011b; etc.).

It is important that in most cases the maximum amplitudes are reached in the S_n group much later than according to the travel-time curve (Fig. 3, (Kopnichev and Arakelyan, 1988; Kaazik and Kopnichev, 1990));

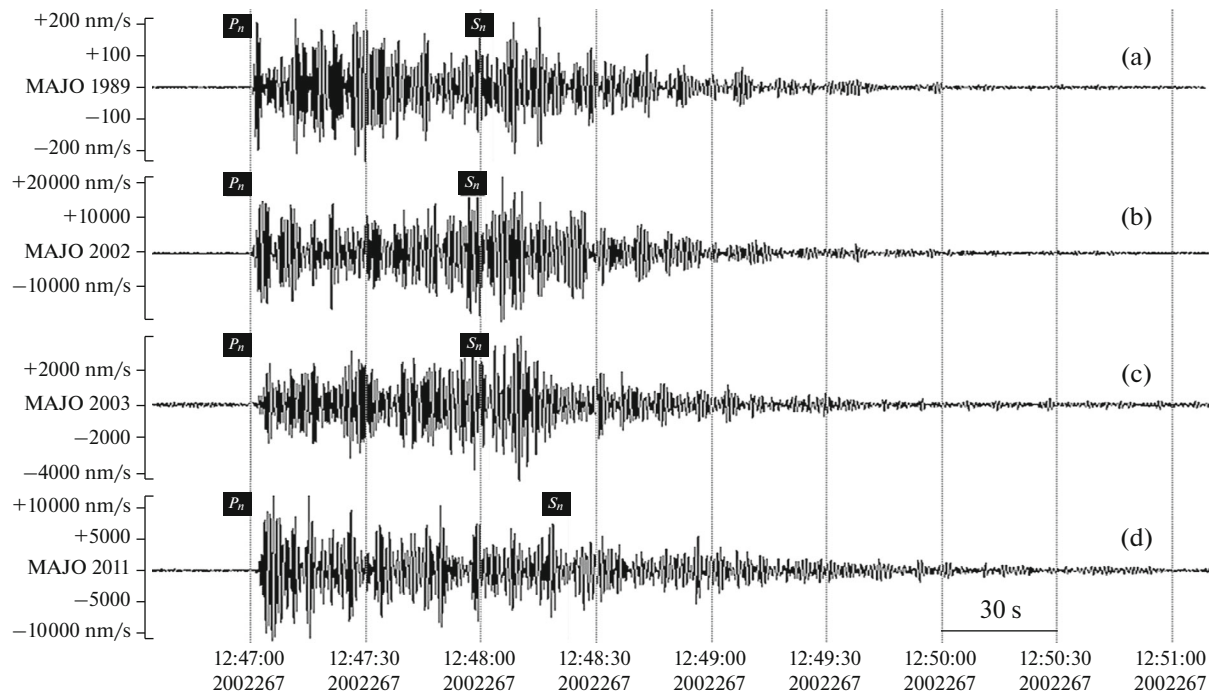


Fig. 3. Examples of the seismograms to illustrate the features of propagation of S_n and P_n waves (MAJO station, vertical component, 1.25 Hz channel). (a) Oct. 12, 1989, 36.55° N, 142.66° E, $h = 33$ km, $\Delta = 399$ km; (b) Sep. 24, 2002, 37.52° N, 142.55° E, $h = 33$ km, $\Delta = 402$ km; (c) Dec. 29, 2003, 38.10° N, 142.35° E, $h = 33$ km, $\Delta = 406$ km; (d) Jun. 14, 2011, 39.48° N, 142.39° E, $h = 20$ km, $\Delta = 491$ km. Moments of P_n and S_n wave arrivals are indicated.

therefore, they cannot correspond to the head wave propagating along the Moho. The set of available data and the results of numerical simulation led us to the conclusion that the maximum amplitudes in the S_n group are related to the shear waves reflected from the numerous subhorizontal boundaries in the upper mantle (Kopnichev and Arakelyan, 1988; Kaazik and Kopnichev, 1990; Kaazik et al., 1990). In this case, when using the records from one station, the level of the S_n group serves as a measure of S -wave attenuation in the lower crust and in the upper mantle in the epicenter area (with respect to the ray deviations (Molnar and Oliver, 1969; Kopnichev and Arakelyan, 1988)). The S_n/P_n parameter is used for normalization, since the S_n and P_n waves propagate along traces that are

close to each other. The data on the characteristics of the attenuation fields and the data obtained by the magnetotelluric sounding method show that the largest content of fluids in the lithosphere of the seismically active regions is recorded in the lower crust and the uppermost mantle (Kvetinskii et al., 1993; Van'yan and Hyndman, 1996; Berdichevskii et al., 1996; Bielinski et al., 2003; Bakirov, 2006). The mean thickness of the Earth's crust in the area of Honshu Island is ~ 30 km. In this case, the length of the segments of the traces passed by the S_n waves in the lower crust in the region under examination is not more than 10–15 km (Yamamoto et al., 2008; Yoshida et al., 2013) and barely depends on Δ ; therefore, the value of the S_n/P_n parameter changes with distance primarily due to the variations in the attenuation in the upper mantle (Fig. 4). Given that the attenuation significantly depends on the wave frequency, the vertical components of the records were preliminarily filtered (a filter with the central frequency of 1.25 Hz and the bandpass of 2/3 octave was used (Kopnichev, 1985)).

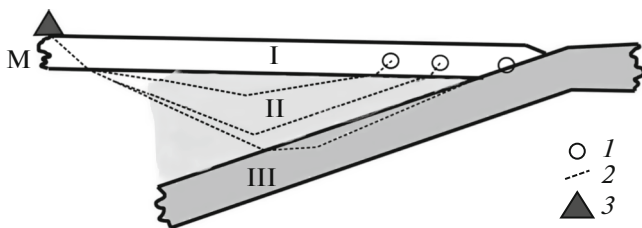


Fig. 4. Scheme of propagation of rays forming the group of S_n waves I continental crust; II mantle wedge; III subducted plate; M Moho. (1) Hypocenters of local earthquakes; (2) assumed traces of rays; (3) seismic station.

DATA ANALYSIS

We divided the area under consideration, including the source zone of the Tohoku earthquake, into four regions limited by the coordinates 36° – 37° , 37° – 38° , 38° – 38° and 39° – $40^\circ 18'$ N; and $140^\circ 30'$ – 145° E. The width of the fourth region was larger in order to com-

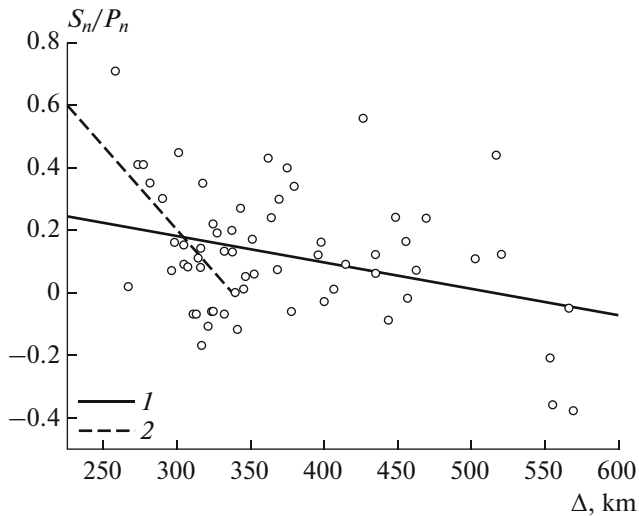


Fig. 5. Distance dependence of S_n/P_n for the 1st region (36–37° N). (1) For all data; (2) at the initial stage of rapid decrease in the S_n/P_n values (at the distances to 340 km, inclusively).

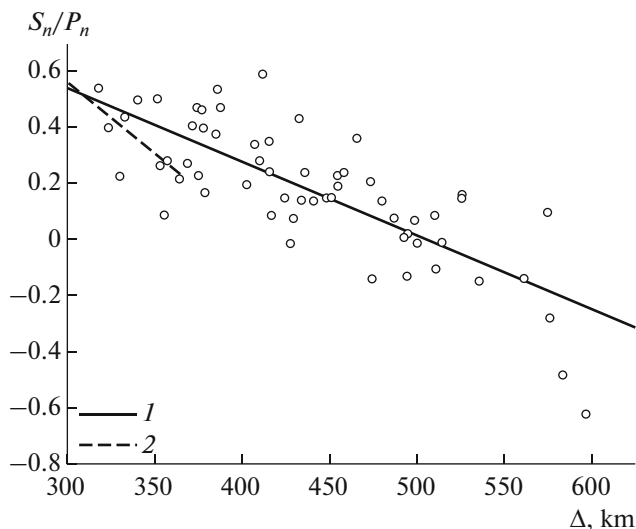


Fig. 6. Distance dependence of S_n/P_n for the 2nd region (37°–38° N). (1) For all data; (2) at the initial stage of rapid decrease in the S_n/P_n values (at the distances to 370 km, inclusively).

pensate the decrease in the data volume due to the growth in the epicentral distances.

Figure 3 shows the typical examples of seismograms for the earthquakes from the indicated regions obtained at the MAJO station at the epicentral distances of 400 to 500 km. It is seen that for all events, the amplitudes of S_n and P_n waves differ by up to a factor of 2; in most cases, the maximum energy in the S_n group is reached significantly later than it arrives by the travel-time curve.

Distance dependences of the S_n/P_n parameter. Figure 5 illustrates the distance dependence of the S_n/P_n parameter for the first (southernmost) region. Most of the points represent the average values obtained for small segments with a linear size, as a rule, of several tens of kilometers. Data averaging makes it possible to decrease the role of the effect of the radiation pattern of the P - and S -waves. It follows from the data presented in Fig. 5 that despite the averaging the data scatter in a broad range. In general, the values of S_n/P_n decrease with distance in the interval $\Delta \sim 250$ –570 km; the equation of linear regression is described by the expression

$$S_n/P_n \sim 0.44 - 0.00085\Delta \text{ (km)}, \quad (1)$$

with a very low correlation factor: $r = -0.33$.

We note that against the background of the general comparatively weak decrease with distance, there are segments of very fast attenuation of the S_n/P_n parameter (in the intervals $\Delta \sim 250$ –340 km and $\Delta \sim 550$ –570 km), as well as a segment of a rather slow decrease in the indicated values (at $\Delta \sim 350$ –520 km). The segment of 550 to 570 km includes the epicenters of the events that occurred in the oceanic plate (down to the ocean trench). In the interval of 250 to 340 km, the correlation dependence has the form

$$S_n/P_n \sim 1.79 - 0.0053\Delta \text{ (km)}, \quad r = -0.59. \quad (2)$$

In addition to this, the values of S_n/P_n show an sharp increase in the narrow interval $\Delta \sim 340$ –375 km (\sim by 0.3 log units on the average).

Figure 6 presents the distance dependence of the S_n/P_n parameter for the second region. Here, the linear regression equation takes the form

$$S_n/P_n \sim 1.33 - 0.0026\Delta \text{ (km)}, \quad (3)$$

$r = -0.79$ (much greater than for the plot in Fig. 5).

In this case, at small distances, the plot of S_n/P_n goes much higher than for the first region; however, this parameter attenuates much faster; therefore, at $\Delta \sim 500$ km, the levels of the correlation dependences become almost identical for both regions. We focus on the segment of a relatively fast decrease in the values of S_n/P_n at distances up to 370 km, for which the equation of regression is described by the expression

$$S_n/P_n \sim 1.99 - 0.0048\Delta \text{ (km)}, \quad r = -0.56. \quad (4)$$

After this segment, the parameter values grow sharply in the interval 370–390 km. Another segment of a fast decrease in the S_n/P_n values is found in the interval $\Delta \sim 550$ –600 km.

Figure 7 shows a similar dependence for the third region that comprises the epicenters of the Tokhoku earthquake and its strongest foreshock (March 9, 2011, $M_w = 7.3$). For this region, the linear regression equation is described by the expression

$$S_n/P_n \sim 1.10 - 0.0022\Delta \text{ (km)}, \quad r = -0.60. \quad (5)$$

It follows from the data presented in Fig. 7 that at the initial segment (in the distance ranging within ~320–450 km), the values of S_n/P_n decrease anomalously fast (by approximately 1.1 log units), and the linear regression equation takes the form

$$S_n/P_n \sim 3.58 - 0.0083\Delta \text{ (km)}, \quad r = -0.69. \quad (6)$$

After that the S_n/P_n parameter increases sharply by 0.5–0.6 log units in the interval of 451 to 480 km. Another segment of a sharp decrease in the S_n/P_n values is found in the distance interval of 600 to 630 km.

Figure 8 illustrates the distance dependence of the S_n/P_n parameter for the fourth (northernmost) region. In this case, the linear regression equation is described by the expression

$$S_n/P_n \sim 0.73 - 0.0017\Delta \text{ (km)}, \quad r = -0.54. \quad (7)$$

It is shown that at the segment of $\Delta \sim 350\text{--}530$ km, the values of S_n/P_n decrease very fast (by 0.9–1.0 log units). Here, the linear regression equation (with a very high correlation coefficient) takes the following form:

$$S_n/P_n \sim 2.31 - 0.0055\Delta \text{ (km)}, \quad r = -0.87. \quad (8)$$

Further, the parameter sharply increases in the interval $\Delta \sim 530\text{--}570$ km by 0.45–0.50 log units. Another segment of a sharp decrease in the S_n/P_n values is found in the interval of $\Delta \sim 600\text{--}700$ km.

Comparison of the plots in Figs. 5–8 shows that at $\Delta \sim 500$ km, the regression line levels are almost the same for the first three regions (0.00–0.03), and for the fourth region, they are slightly lower (–0.12). We note also that the greatest contrast of the S_n/P_n values at a small change in the epicentral distance corresponds to the third region.

Figure 9 presents the common plot of $S_n/P_n(\Delta)$ for the whole source zone of the Tohoku earthquake. In this case, the correlation dependence is described by the expression

$$S_n/P_n \sim 0.83 - 0.00167\Delta \text{ (km)}, \quad r = -0.57. \quad (9)$$

For comparison, Fig. 9 illustrates the correlation dependence of the S_n/P_n parameter on the distance for the source zone of the strongest Maule earthquake of February 27, 2010 (Chili, $M_w = 8.8$). We analyzed the records of the seismograms obtained at the PLCA station for the traces passing in the area between 33° and 41° S (Kopnischev and Sokolova, 2011b). The regression line in the interval of ~300–850 km is described by the dependence

$$S_n/P_n \sim 1.27 - 0.00143\Delta \text{ (km)}. \quad (10)$$

It is seen that at $\Delta \sim 500$ km, the plot level for the zone of the Maule earthquake is above dependence (9) by 0.58 log units (the deviation is greater than 2σ).

Characteristics of the attenuation field. Figures 10–13 present the inhomogeneities of the S-wave attenuation field for four regions. All values of S_n/P_n are divided

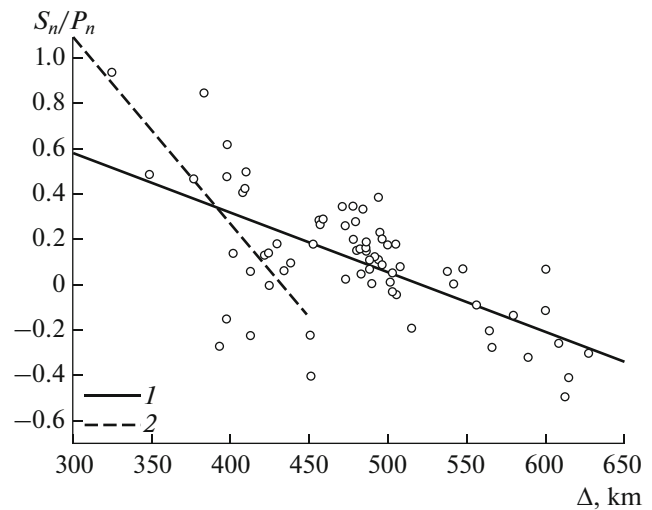


Fig. 7. Distance dependence of S_n/P_n for the 3rd region (38°–39° N). (1) For all data; (2) at the initial stage of rapid decrease of the S_n/P_n values (at the distances to 451 km, inclusively).

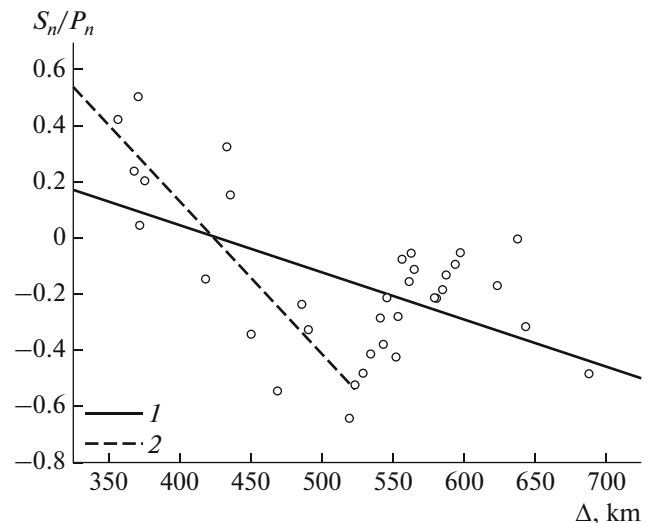


Fig. 8. Distance dependence of S_n/P_n for the 4th region (39°–40.3° N). (1) For all data; (2) at the initial stage of rapid decrease of the S_n/P_n values (at the distance to 530 km, inclusively).

into three groups corresponding to the low, intermediate, and high attenuation. Low attenuation takes place when the values of S_n/P_n deviate from dependences (1), (3), (5), and (7) by more than 0.15 log units; intermediate attenuation takes place, when the values deviate by up to ± 0.15 ; and high attenuation takes place, when the values deviate below -0.15 log units. It follows from the data in Fig. 10 that the brightest features of the attenuation field in the first region are the two submeridional bands of low values of the S_n/P_n parameter between meridians 141.5° and 142° E and along merid-

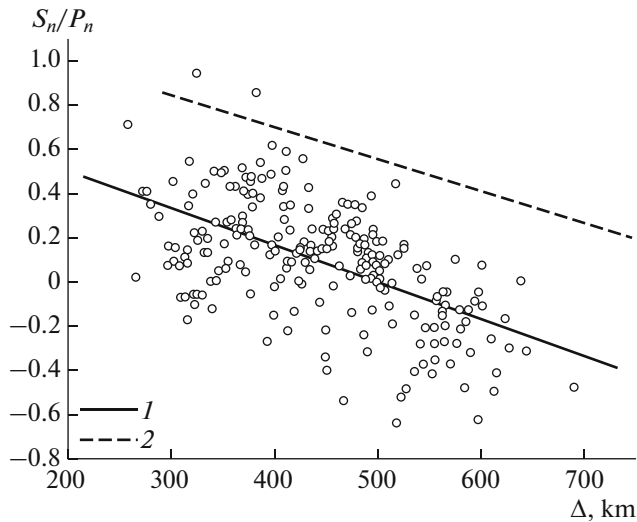


Fig. 9. (1) Distance dependence of S_n/P_n on the whole data set and (2) same dependence for the source zone of the Maule earthquake (Chile, February 27, 2010) February 27, 2010).

ian 144.5° E, respectively. At the same time, the area of the trench and its nearest vicinity displays primarily intermediate and low attenuation.

In the second region, the attenuation, which shows two sublateral bands of the high and low values of the S_n/P_n parameter northward of parallel 37.5° N, is mostly intermediate (Fig. 11).

Figure 12 illustrates the inhomogeneities of the attenuation field in the third region. We identified here a small segment of comparatively high values of S_n/P_n near the volcanic front. At the same time, a small spot of low values of the parameter lies on the coast of Honshu Island. An extensive submeridional band of low S_n/P_n values is recorded along the meridian 142.5° E. We note that between meridians 142.0° and 142.6° E, there is the strongest contrast segment of $\sim 0.5^\circ \times 0.5^\circ$, where for 15–20 km the S_n/P_n parameter decreases sharply by 0.5–0.7 log units. It is important that the epicenter of the main Tohoku earthquake is found at this segment. In addition, between the meridians 142.0° and 142.3° E, there lies a narrow deep ring seis-

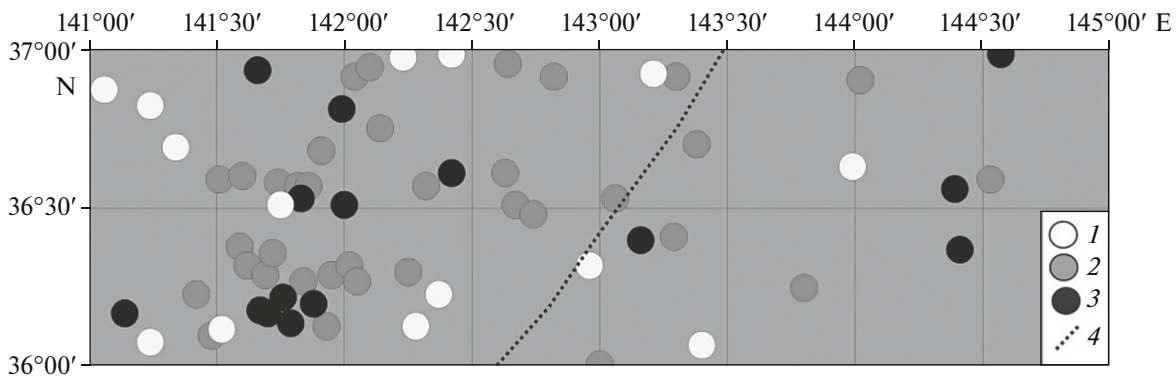


Fig. 10. Inhomogeneities in the S -wave attenuation field in the upper mantle of the 1st region (36° – 37° N). (1–3) Attenuation: (1) low; (2) intermediate; (3) high; (4) the Japan Trench axis.

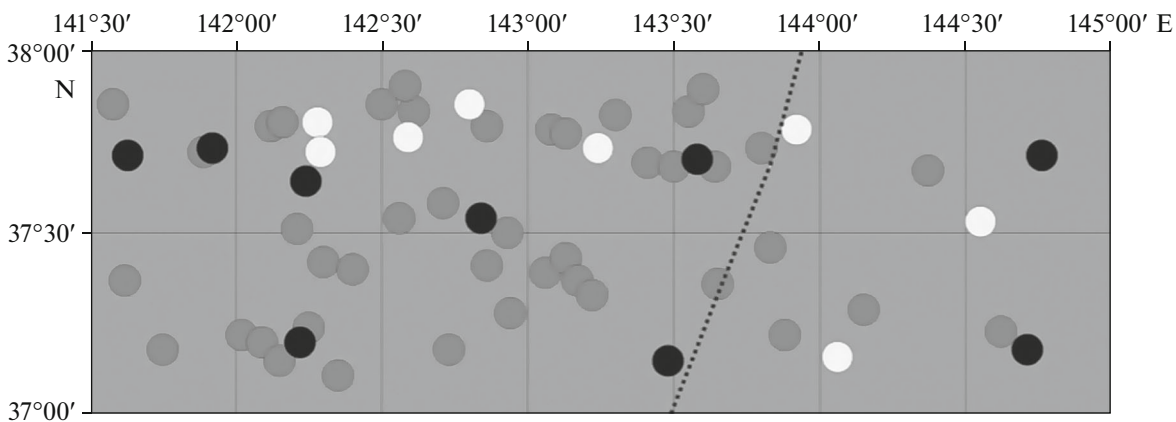


Fig. 11. Inhomogeneities in the S -wave attenuation field in the upper mantle of the 2nd region (37° – 38° N). Designations are given in Fig. 10.

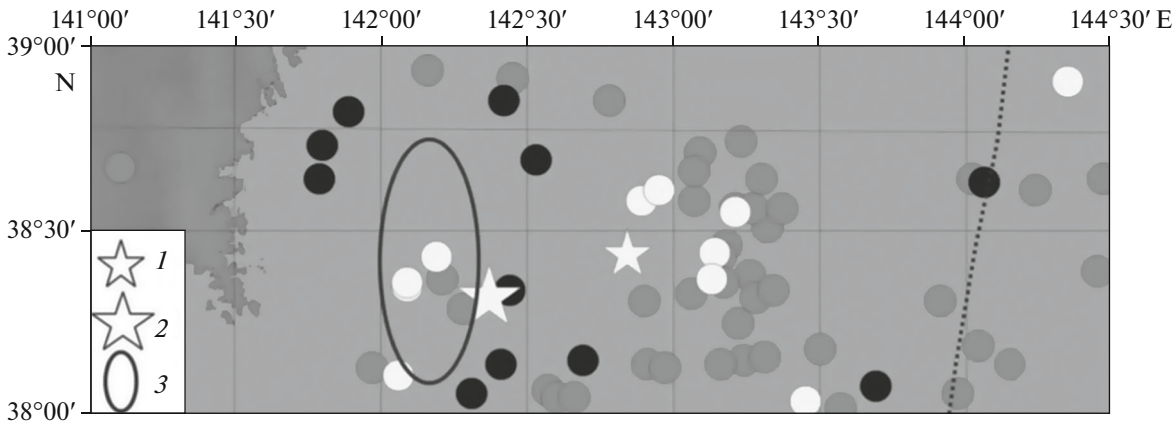


Fig. 12. Inhomogeneities in the S -wave attenuation field in the upper mantle of the 3rd region (38° – 39° N). (1, 2) Epicenters for (1) the strong foreshock of March 3, 2011 ($M_w = 7.3$); (2) the major earthquake of March 11, 2011; (3) deep ring structure (Kopnischev and Sokolova, 2012). The rest of the designations are given in Fig. 10.

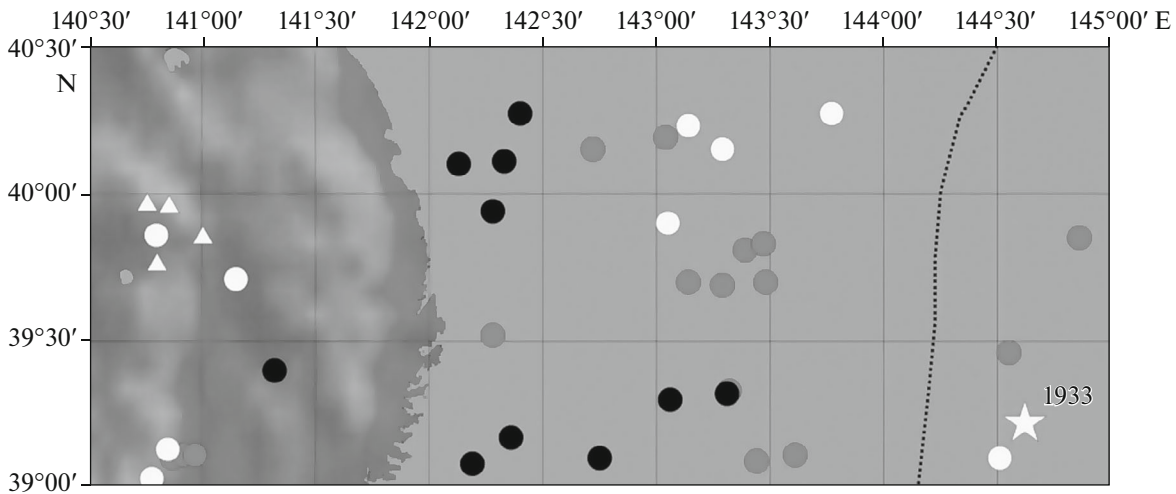


Fig. 13. Inhomogeneities in the S -wave attenuation field in the upper mantle of the 4th region. Conventional symbols are indicated in Fig. 1 (volcanos) and Fig. 10.

micity structure ($h = 34$ – 70 km) with the threshold value $M_{\text{thresh}} = 5.4$, which had been formed for 35 years before the great earthquake (Kopnischev and Sokolova, 2012). Another less contrasting segment, at which the values of S_n/P_n significantly increase, is found between meridians 142.5° and 143.2° E. It is interesting that the epicenter of the strongest foreshock of the Tohoku earthquake lies in this segment (March 9, 2011, $M_w = 7.3$).

Figure 13 illustrates the inhomogeneities of the attenuation field in the fourth region. Here, we delineate a segment of relatively weak attenuation in the east of Honshu Island, for which the ray traces move mostly in the volcanic zone. The values of S_n/P_n are mostly low in the coastal zone between 142.0° and 142.5° E; the sublateral band of high attenuation is observed in the south of the region between 142.0° and

143.5° E, and the segment of weak attenuation is recorded in the north between 143° and 144° E.

DISCUSSION

The vivid characteristic of the plots presented in Figs. 5–8 is that the initial segments of the more-or-less fast decrease in the values of S_n/P_n change to short segments of rapid growth in their values. We note first that the indicated effects make it possible to additionally specify the nature of the group of S_n waves. It is evident that the existence of the segments of the sharp increase in the values of S_n/P_n after the intervals of their fast decrease cannot be explained if we consider that the S_n group represents the head waves propagating in the upper mantle along the M boundary. This conclusion was made earlier in (Molnar and Oliver,

1969; Kopnichev and Arakelyan, 1988; Kaazik and Kopnichev, 1990) based on the analysis of the available data set and on the results of numerical simulation. At the same time, the new data are consistent with the model of the formation of the S_n group by the shear waves reflected from the numerous subhorizontal boundaries in the upper mantle (Kopnichev and Arakelyan, 1988; Kaazik and Kopnichev, 1990). It follows from the scheme (Fig. 4) that in this case, the increase in the S_n/P_n parameter is explained simply by the passage of the rays to the region of weak attenuation of the S -waves in the upper mantle from the region of high attenuation.

In principle, the high attenuation of the shear waves can be related to the increased content of molten rocks or fluids. However, as follows from the data presented in Figs. 12 and 13, the traces at small distances from the third and fourth regions (mostly, along the volcanic zone) are dominated by quite high values of S_n/P_n , which indicates relatively weak attenuation. Consequently, we may assume that in our case the high attenuation of the S -waves is determined primarily by the increase in the share of free fluids in the upper mantle.

Most of the epicenters of the events for which the S_n/P_n parameter was estimated are located between the volcanic front and the ocean trench. At short epicentral distances, the traces of the rays for such events move in the uppermost parts of the mantle in the region of the mantle wedge (Yamamoto et al., 2008; Yoshida et al., 2013). It follows from the data in Figs. 10, 12, and 13 that the weak attenuation of the S -waves occurs in the first, third, and fourth regions. At an increase in Δ , the rays sink deeper; moreover, initially, the attenuation decreases regularly, which indicates an increase in the share of free fluids at great depths. It is well known that the main source of fluids rising to the mantle wedge is the dehydration of the crust of the subsiding oceanic plate, for which reason their highest content corresponds to the lower part (bottom) of the wedge that borders the plate (Wada et al., 2008). Hence, the smallest values of S_n/P_n at the initial segment of the decrease in this parameter are most likely to correspond to the rays falling on the bottom of the mantle wedge. At the same time, at a further increase in Δ , the rays penetrate into the subsiding Pacific Plate, which is characterized by high velocities and very weak attenuation (Yamamoto et al., 2008; Yoshida et al., 2013). A fast decrease in the share of the trace passing along the bottom of the mantle wedge and the increase in the share of the trace passing along the plate with a much higher Q -factor lead to a significant decrease in the integral attenuation and growth of the S_n/P_n parameter. Thus, we may assume that the main features of the distance dependences of the S_n/P_n parameters are determined first of all by the wave propagation in a very inhomogeneous medium that is characterized by an anomalously high contrast of the

S -wave attenuation on the bottom of the mantle wedge and on the roof of the subducting plate. We note that another segment of rapid decrease in the S_n/P_n values at relatively large distances is likely to be related to the rays falling in a waveguide: the zone of dehydration of mantle rocks in the lower part of the Pacific Plate (Yamasaki and Seno, 2003).

Note that the epicenters of the main earthquake of March 11, 2011 and its strongest foreshock are found in the third region, which is characterized by the greatest contrast of the S_n/P_n values at comparatively short distances. In addition, this region contains a deep ring seismicity structure (at depths of 34 to 70 km), which had been formed for a few decades before the Tohoku earthquake (Kopnichev and Sokolova, 2012). The epicenter of the strongest event was located near this structure, which is recorded also for the epicenters of many other large earthquakes in different zones of subduction (Kopnichev and Sokolova 2011b, 2018). This effect is related to the greatest thickness of the two-phase layer and the concentration of stresses on its roof (in the case when there are connecting pores and fractures filled with a fluid) (Karakin and Lobkovskii 1982; Gold and Soter, 1984/1985), which can be a trigger leading to the occurrence of strong and the strongest events. In this regard, we note that the hypocenter of the Tohoku earthquake was located at a depth of 32 km, i.e., almost on the roof of the deep ring structure. Thus, the characteristics of the attenuation field and the seismicity data are consistent with each other; they indicate that the fluid content is the highest in the upper mantle of the third region between 142.0° and 142.5° E (with respect to the deviation of the S_n group rays).

It was shown earlier in (Husen and Kissling, 2001; Kopnichev and Sokolova, 2003, 2009; Ogawa and Heki, 2007) that, after the numerous strong and great earthquakes in the interplate regions, there was a rise in the fluid from the upper mantle into the Earth's crust, including its upper part, for several decades. The low density of fluids provides a release of high potential energy as a result of their rise. We suggested the hypothesis that the energy of strong seismic events is proportional to the potential energy released when the fluids in the source zone ascend (Kopnichev and Sokolova, 2018). It was indicated in that work that the size of the ring seismicity structures formed before strong and the great earthquakes in the subduction zones is significantly greater in the east than in the west of the Pacific Ocean, with the other conditions being the same. At the same time, the threshold values of the magnitudes of the events forming ring structures are close to each other in two large regions of the Pacific Ring. The available data show that the formation of the ring structures is related to the migration of deep-seated fluids at depths down to 70 km (Kopnichev and Sokolova, 2010a, 2011b, 2012, 2018). Taking into account the possible proportionality of the energy of

large earthquakes to the potential fluid energy, we consider that the specific content of the liquid phase in the lithosphere of the subduction zones in the east of the Pacific Ocean is much lower than in the west (Kopnichev and Sokolova, 2018). We verified the fairness of such a statement by analyzing the characteristics of the short-period *S*-wave attenuation fields.

The data obtained here and earlier (Kopnichev and Sokolova, 2011b) allow comparing the characteristics of the attenuation fields in the rather large source zones of the two recent great earthquakes with magnitudes close to each other, one of which occurred on the northwestern and the second on the southeastern margins of the Pacific Ocean. This comparison is the most correct one, since as stated above, the attenuation of *S*-waves in the source zones gradually decreased for several decades after the strong and strongest events (Kopnichev et al., 2009). It follows from the data in Fig. 9 that in general the attenuation of *S*-waves in the subduction zone of the Pacific Plate in the northeast of Japan is significantly higher than in the subduction zone of the Nazca Plate that sinks under the South American continent (between 33° and 41° S) (Kopnichev and Sokolova, 2011b). Thus, the data obtained confirm our previous conclusion about the much greater content of fluids in the subduction zones in the west of the Pacific Ocean compared to the east.

As we noted, the hydrated rocks in the subducting oceanic plates are the source of the fluids in the subduction zones. It is well known that the share of hydrated rocks increases as the age of subducted plates grows (Yamasaki and Seno, 2003). The data on the characteristics of the attenuation field are consistent with the much older age of the ancient Pacific Ocean Plate in the northeast of Japan (~130 Ma (Nakanishi et al., 1992)) compared to the relatively young Nazca Plate subducting under the South American continent (~50 Ma (Yamasaki and Seno, 2003)).

The new data are also correlated with the earlier results of analyzing the aftershock processes in the subduction zones along the periphery of the Pacific Ocean. It was shown in (Singh and Suarez, 1988) that the number of aftershocks of the large earthquakes is significantly higher for the events in the west of the Pacific Ocean than in the east, with the other conditions being the same. In addition to this, it was determined in (Tajima and Kanamori, 1985) that the aftershock zones of the large earthquakes spread out with time more in the western part of the Pacific Ocean than in the eastern part. We may assume that these effects are related to the following circumstances. The data obtained in the past two decades indicate that the fluids in the subduction zones rise from the upper mantle primarily due to the earthquakes (Husen and Kissling, 2001; Yamazaki and Seno, 2003; Kopnichev and Sokolova, 2005; Ogawa and Heki, 2007; Kopnichev et al., 2009). Therefore, the larger number of

aftershocks, including the rather strong ones, facilitates the drying of the fluid-saturated upper mantle in the west of the Pacific Ocean. At the same time, the rise of the fluids from the less humid upper mantle of the east of the Pacific Ocean requires fewer aftershocks.

At the same time, the greater expansion of the aftershock zones with time in the west of the Pacific Ocean is more likely determined by the more active migration of the large quantity of fluids that rose to the Earth's crust in the horizontal direction. Such effects were established earlier for the source zones of several large earthquakes in the intracontinental areas (Rojstaczer and Wolf, 1992; Kopnichev and Sokolova, 2004, 2005).

CONCLUSIONS

The characteristics of the short-period *S*-wave attenuation fields in the source zone of the strongest Tohoku earthquake of March 11, 2011 ($M_w = 9.0$) are presented. The records of shallow local earthquakes obtained at the MAJO station at distances of 250 to 700 km were processed. The method based on the analysis of the ratio between the maximum amplitudes of the S_n and P_n waves (the S_n/P_n parameter) was used. The source zone was divided into four regions bounded by coordinates 36°–37°, 37°–38°, 38°–39°, and 39°–40°18' N; and 140°30'–145° E. It was established that at small epicentral distances all regions contain segments of a fast decrease in the S_n/P_n values that changed to segments of sharp growth. Another segment of rapid decrease in the S_n/P_n parameter is identified in all regions at relatively large distances. It is assumed that the first segments of the rapid decrease in the S_n/P_n values are related to the gradual penetration of the *S*-wave rays into the mantle wedge. In this case, the minimum values of the parameter correspond to the rays partly moving along the foot of this wedge. This effect is explained by the fact that the lower part of the mantle wedge corresponds to the largest content of deep-seated fluids rising as a result of the dehydration of rocks of the oceanic crust. The segments of the sharp growth in the S_n/P_n values more likely to correspond to the ray propagation in the upper part of the plate characterized by very weak attenuation. The second segments of the fast decrease in the S_n/P_n parameter are associated with the penetration of the rays into the waveguide formed in the lower part of the plate as a result of the dehydration of the mantle rocks. The average values of S_n/P_n (Δ) are much lower in all four regions than in the source zone of the strongest Maule earthquake (Chile, February 27, 2010, $M_w = 8.8$). This effect is consistent with the previous assumption about the larger content of fluids in the subduction zone in the west of the Pacific Ocean compared to the east. This also makes it possible to explain the features of the aftershock processes in two large regions of the Pacific Ring.

CONFLICT OF INTEREST

The authors declare that they have no conflict of interest.

REFERENCES

- Bakirov, A.B., *Zemnaya kora i verkhnyaya mantiya Tyan'-Shanya v svyazi s geodinamikoi i seismichnost'yu* (The Earth's Crust and Upper Mantle of the Tien Shan Associated with Geodynamics and Seismicity), Bishkek: Ilim, 2006.
- Berdichevskii, M.N., Borisova, V.P., Golubtsova, N.S., et al., Interpretation of magnetotelluric soundings in the Lesser Caucasus, *Izv., Phys. Solid Earth*, 1996, vol. 32, no. 4, pp. 365–370.
- Bielinski, R., Park, S., Rybin, A., Batalev, V., Jun, S., and Sears, C., Lithospheric heterogeneity in the Kyrgyz Tien Shan imaged by magnetotelluric studies, *Geophys. Res. Lett.*, 2003, vol. 30, no. 15. <https://doi.org/10.1029/2003GL017455>
- Furumura, T. and Kennett, B., Variations in regional phase propagation in the region around Japan, *Bull. Seismol. Soc. Am.*, 2001, vol. 91, pp. 667–682.
- Gold, T. and Soter, S., Fluid ascent through the solid lithosphere and its relation to earthquakes, *Pure Appl. Geophys.*, 1984, vol. 122, nos. 2–4, pp. 492–530.
- Goldfinger, C., Yeats, R., Ikeda, Y., and Ren, J., Superquakes and supercycles, *Seismol. Res. Lett.*, 2013a, vol. 84, no. 1, pp. 24–32.
- Goldfinger, C., Ikeda, Y., and Yeats, R., Superquakes, supercycles and global earthquake clustering, *Earth*, 2013b, vol. 58, no. 1, p. 34.
- Husen, S. and Kissling, E., Postseismic fluid flow after the large subduction earthquake of Antofagasta, Chile, *Geology*, 2001, vol. 29, no. 9, pp. 847–850.
- Kaazik, P.B. and Kopnichev, Yu.F., Numerical simulation of the group S_n and codes in a medium that is inhomogeneous by velocity and absorption, *Vulkanol. Seismol.*, 1990, no. 6, pp. 74–87.
- Kaazik P.B., Kopnichev, Yu.F., Nersesov, I.L., and Rakhmatullin, M.Kh., Analysis of the fine structure of short-period seismic fields by station groups, *Fiz. Zemli*, 1990, no. 4, pp. 38–49.
- Karakin, A.V. and Lobkovskii, L.I., The hydrodynamics and structure of a two-phase asthenosphere, *Dokl. Akad. Nauk SSSR*, 1982, vol. 268, no. 2, pp. 324–329.
- Kopnichev, Yu.F., *Korotkoperiodnye seismicheskie volnovye polya* (Short-Period Seismic Wave Fields), Moscow: Nauka, 1985.
- Kopnichev, Yu.F. and Arakelyan, A.R., On the nature of short-period seismic fields at distances less than 3000 km, *Vulkanol. Seismol.*, 1988, no. 4, pp. 77–92.
- Kopnichev, Yu.F. and Sokolova, I.N., Spatiotemporal variations of the S -wave attenuation field in the source zones of large earthquakes in the Tien Shan, *Izv., Phys. Solid Earth*, 2003, vol. 39, no. 7, pp. 568–579.
- Kopnichev, Yu.F. and Sokolova, I.N., Spatiotemporal variations of the S -wave attenuation field in source zones of large earthquakes in the Tien Shan region: Evidence from the records of underground nuclear explosions, *Dokl. Earth Sci.*, 2004, vol. 395, no. 3, pp. 461–464.
- Kopnichev, Yu.F. and Sokolova, I.N., Rise of mantle fluids in areas of sources of large earthquakes and large fault zone: Geochemical evidence, *Vestn. NYaTs RK*, 2005, no. 2, pp. 147–155.
- Kopnichev, Yu.F. and Sokolova, I.N., Heterogeneities in the field of short period seismic wave attenuation in the lithosphere of central Tien Shan, *J. Volcanol. Seismol.*, 2007, vol. 1, no. 5, pp. 333–348.
- Kopnichev, Yu.F. and Sokolova, I.N., On the correlation between seismicity characteristics and S -wave attenuation in the ring structures that appear before large earthquakes, *J. Volcanol. Seismol.*, 2010a, vol. 4, no. 6, pp. 396–411.
- Kopnichev, Yu.F. and Sokolova, I.N., Heterogeneities in the absorption field of short-period S waves in the lithosphere of Tien Shan and Dzungaria with their relation to seismicity, *Dokl. Earth Sci.*, 2010b, vol. 433, no. 2, pp. 1119–1123.
- Kopnichev, Yu.F. and Sokolova, I.N., Heterogeneities of the field of short-period shear wave attenuation in the lithosphere of Central Asia and their relationship with seismicity, *Dokl. Earth Sci.*, 2011a, vol. 437, no. 1, pp. 363–367.
- Kopnichev, Yu.F. and Sokolova, I.N., Inhomogeneities in the field of absorption of short-period S -waves near the source of the Maule earthquake (Chile, February 27, 2010, $M_w = 8.8$) and their relation to seismicity and volcanism, *Geofiz. Issled.*, 2011b, vol. 12, no. 3, pp. 22–33.
- Kopnichev, Yu.F. and Sokolova, I.N., Ring structures of seismicity in northeastern Japan and the catastrophic Tohoku earthquake of 11 March 2011 ($M_w = 9.0$), *Vestn. Nats. Yad. Tsentra Resp. Kaz.*, 2012, no. 1, pp. 121–130.
- Kopnichev, Yu.F. and Sokolova, I.N., High S -wave attenuation anomalies and ringlike seismogenic structures in the lithosphere beneath Altai: Possible precursors of large earthquakes, 2016, *Izv., Atmos. Ocean. Phys.*, 2016, vol. 52, no. 8, pp. 806–815.
- Kopnichev, Yu.F. and Sokolova, I.N., Ring-shaped seismicity structures in the cascadia subduction zone: Possible upcoming large earthquakes, *Izv., Atmos. Ocean. Phys.*, 2018, vol. 54, no. 7, pp. 745–752. <https://doi.org/10.1134/S0001433818070046>
- Kopnichev, Yu.F., Gordienko D.D., and Sokolova, I.N., Space–time variations of the shear wave attenuation field in the upper mantle of seismic and low seismicity areas, *J. Volcanol. Seismol.*, 2009, vol. 3, no. 1, pp. 44–58.
- Kvetinskii, S.I., Kopnichev, Yu.F., Mikhailova, N.N., Nurmagametov, A.N., and Rakhmatullin, M.Kh., Inhomogeneities of the lithosphere and asthenosphere in the source zones of large earthquakes in the northern Tien Shan, *Dokl. Ross. Akad. Nauk*, 1993, vol. 329, no. 1, pp. 25–28.
- Molnar, P. and Oliver, J., Lateral variations of attenuation in the upper mantle and discontinuities in the lithosphere, *J. Geophys. Res.*, 1969, vol. 74, pp. 2648–2682.
- Nakanishi, M., Tamaki, K., and Kobayashi, K., A new Mesozoic isochron chart of the northwestern Pacific ocean: Paleomagnetic and tectonic implications, *Geophys. Res. Lett.*, 1992, vol. 19, pp. 693–696.
- Ni, J. and Barazangi, M., High-frequency seismic wave propagation beneath the Indian shield, Tibetan plateau and surrounding regions: High uppermost mantle ve-

- locities and efficient S_n propagation beneath Tibet, *Geophys. J. R. Astron. Soc.*, 1983, vol. 72, pp. 665–689.
- Ogawa, R. and Heki, K., Slow postseismic recovery of geoid depression formed by the 2004 Sumatra–Andaman earthquake by mantle water diffusion, *Geophys. Res. Lett.*, 2007, vol. 34, L06313.
- Rojstaczer, S. and Wolf, S., Permeability changes associated with large earthquakes: An example from Loma Prieta, California, *Geology*, 1992, vol. 20, pp. 211–214.
- Singh, S. and Suarez, G., Regional variation in the number of aftershocks ($m_b \geq 5$) of large subduction-zone earthquakes ($M_w \geq 7.0$), *Bull. Seismol. Soc. Am.*, 1988, vol. 78, no. 1, pp. 230–242.
- Tajima, F. and Kanamori, H., Global survey of aftershock area expansion, *Phys. Earth. Planet. Inter.*, 1985, vol. 40, pp. 77–134.
- Van'yan, L.L. and Hyndman, R.D., On the origin of electrical conductivity in the consolidated crust, *Izv., Phys. Solid Earth*, 1996, no. 4, pp. 268–284.
- Wada, I., Wang, K., He, J., and Hyndman, R., Weakening of the subducting interface and its effects on surface heat flow, slab dehydration and mantle wedge serpentinization, *J. Geophys. Res.*, 2008, vol. 113, B04402. <https://doi.org/10.1029/2007JN005190>
- Yamamoto, Y., Hino, R., Suzuki, K., Ito, Y., et al., Spatial heterogeneity of the mantle wedge structure and interplate coupling in the NE Japan region, *Geophys. Res. Lett.*, 2008, vol. 35, L23304. <https://doi.org/10.1029/2008GL036100>
- Yamasaki, T. and Seno, T., Double seismic zone and dehydration embrittlement of the subducting slab, *J. Geophys. Res.*, 2003, vol. 108, no. B4. <https://doi.org/10.1029/2002JB001918>
- Yoshida, T., Kimura, J., Yamada, R., Acocella, V., et al., Evolution of late Cenozoic magmatism and the crust–mantle structure in the NE Japan arc, *Geol. Soc. London: Spec. Publ.*, 2013, vol. 385, pp. 335–387.
- Zhao, C., Kennett, B., and Furumura, T., Contrasts in regional seismic wave propagation to station WMQ in Central Asia, *Geophys. J. Int.*, 2003, vol. 155, pp. 44–56.

Translated by L. Mukhortova